DOI 10.5012/bkcs.2010.31.04.1004

Structural Studies of the Self-Assemblies Created with Dipyrrins

Ji-Young Shin, Brian O. Patrick, Seung Bae Son,† Jae Ryang Hahn,† and David Dolphin*

Department of Chemistry, University of British Columbia, 2036 Main Mall, Vancouver B.C. V6T 1Z1, Canada
**E-mail: david.dolphin@ubc.ca*
†Department of Chemistry, Chonbuk National University and Research Institute of Physics and Chemistry, Jeonju 561-756, Korea
Received December 15, 2009, Accepted January 23, 2010

Three-dimensional superstructures of unique self-assemblies generated by exploring the conformational flexibility of various dipyrromethenes through creation of hydrogen-bonds with metal-halide anions are reported and the conformational diversity is thoroughly described in the solid and solution states by X-ray diffraction analysis and variable temperature NMR spectroscopy. The tetrahedral or octahedral structures of their precursors, various metal-dipyrromethene complexes, are also reported, based on the crystallographic data. STM images of the self-assemblies observed on graphite surfaces present interesting arrangements and appear as tubular bunches.

Key Words: Dipyrromethene, Metal complex, Hydrogen-bond, STM

Introduction

The chemistry of inter/intramolecular interactions that result in the self-assembly of supramolecules is attracting considerable interest in many diverse areas of chemistry, physics, engineering and crystal design.[1-11] Self-assemblies of supramolecules may be formed *via* weak inter/intramolecular interactions such as metal-organic, hydrogen-bonding, electrostatic and hydrophobic interaction and van der Waals interactions. The fact that metal-ligand interactions (20 - 80 kcal/mole) are smaller than covalent bond strengths, which are typically 100 kcal/mole, allows for many different ligands to be introduced into self-assemblies. Over the past decade, porphyrins and related polypyrrolyl analogues have been examined as interesting building blocks for self-assemblies due to their versatile metal-coordination capacities.[12-16] Alternatively, hydrogen-bonding and electrostatic and hydrophobic interactions which are typically less than 10 kcal/mole in general, are also important factors in the formation of self-assemblies. Unique 3-dimensional self-assembled structures generated through inter/intramolecular hydrogen-bonding interactions can be expected when using polypyrrolyl analogues having amino-type and imino-type nitrogens (or other strong hydrogen-bond-acceptors such as oxo-substituents).[17-21] A class of "supramolecular synthons[22-23]" containing both hydrogen-bonding donors and acceptors can lead to the creation of diverse types of new self-assemblies through hydrogen-bonding networks, which control the packing of the "molecular tectons".[24-26]

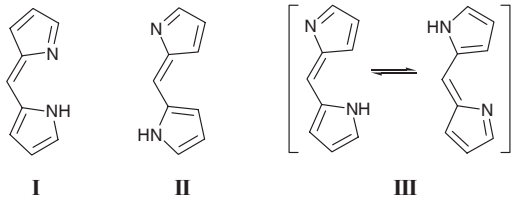

Figure 1. Three possible configurations of dipyrromethene.

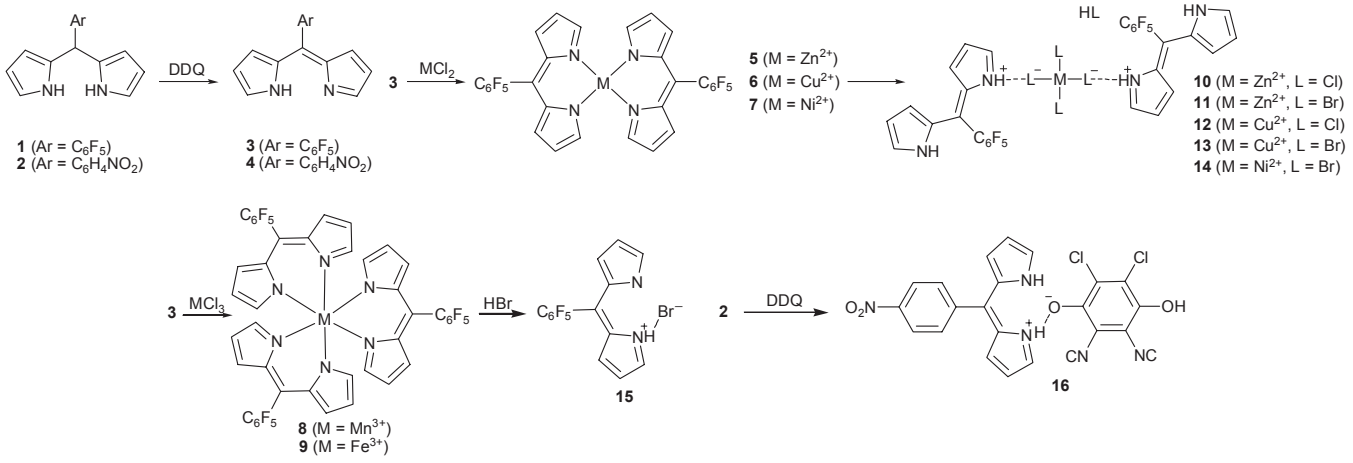

Scheme 1. Synthetic process

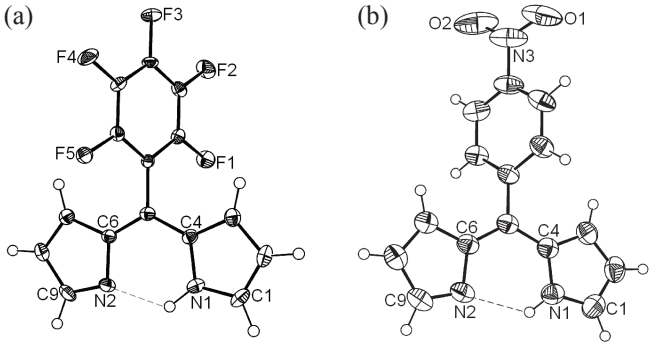

Figure 2. Crystal structures of dipyrromethenes (a) **3** and (b) **4**.[29]

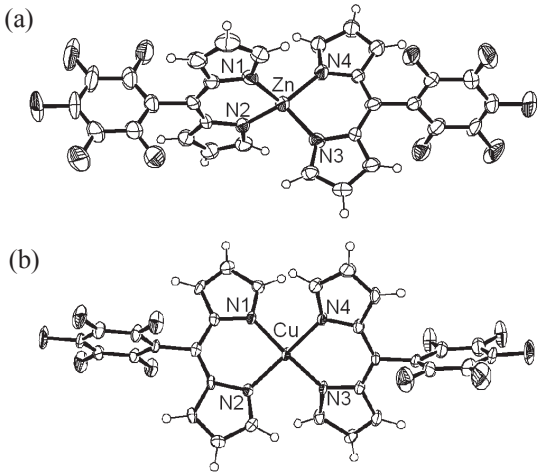

Figure 3. Crystal structures of (a) Zn^{2+} dipyrromethene **5** and (b) Cu^{2+} dipyrromethene **6**.

Dipyrrins exhibit rotations of the pyrrolyl groups around the central methene-bridge and three different conformations are expected (types **I**, **II** and **III** in figure 1).[27] Recently, we reported several unique self-assemblies in which protonated dipyrrins were crystallized with metal-halide anions.[28] When dipyrrins form crystals of various self-assemblies with secondary components, the conformational dynamics of the dipyrrin components play a key role. Consequently, the electronic features of the dipyrrin components affect these dynamics. Dipyrrins **3** and **4** (Scheme 1), which contain electron-withdrawing groups on the meso-aryls and are unsubstituted in the α-positions, are chemically stable and conformationally mobile. In this respect, **3** and **4** have been suggested as good candidates for incorporation into further structures.

Free-base dipyrrins and metal-dipyrrin complexes exist mostly in the type **I** form *via* intramolecular hydrogen-bonding between imino- and amino-N atoms and ligand-metal chelation (see Figures 2-4). Dicationic metal complexes of **3**, ZnD_2 **5** and CuD_2 **6** (having a 1:2 binding ratio for metal and dipyrrins to form tetrahedral complexes) and tricationic metal complexes of **3**, MnD_3 **8** and FeD_3 **9** (having 1:3 binding as a result of octahedral coordination) have been prepared. All of their crystal structures reveal type **I** conformation of the dipyrrin moiety.

When the metal complexes (**5**-**7**) were treated with hydrogen

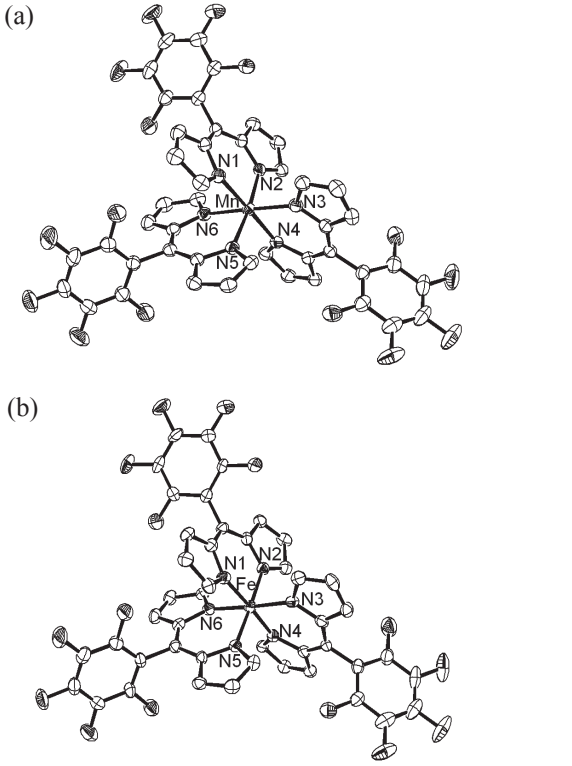

Figure 4. Crystal structures of (a) Mn^{3+} dipyrromethene **8** and (b) Fe^{3+} dipyrromethene **9**; H-atoms have been omitted for clarity.

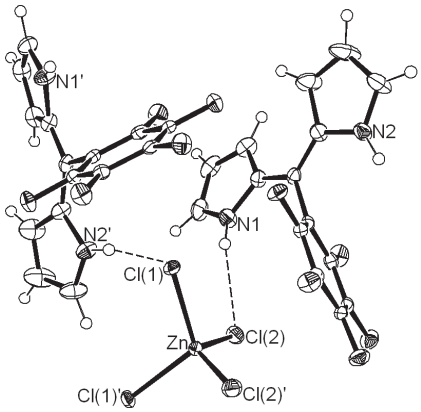

Figure 5. ORTEP structure[28] of **10**.

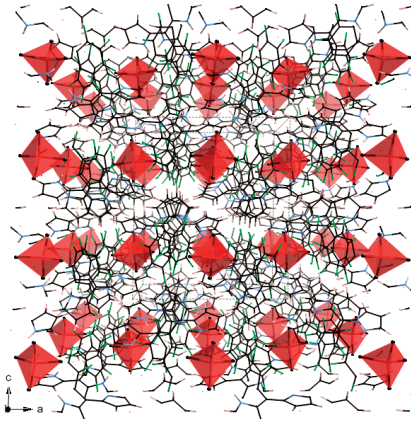

Figure 6. 3D-packing diagram of **10**.

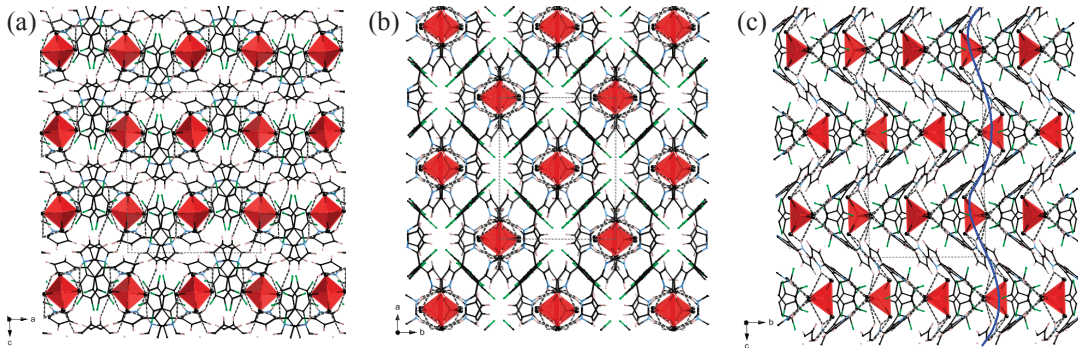

Figure 7. Packing diagrams of **10** through each side; (a) ac, (b) ab, and (c) bc planes. Hydrogen-bonds have been displayed as dotted lines.

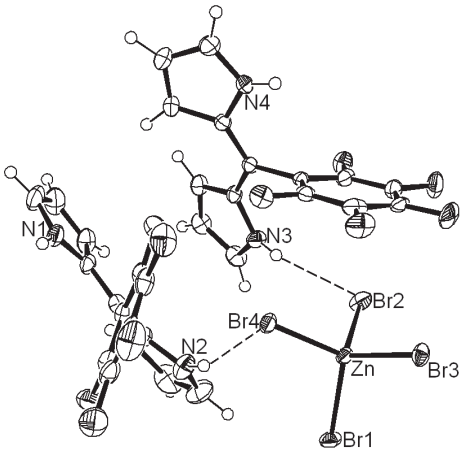

Figure 8. ORTEP structure[28] of **11**.

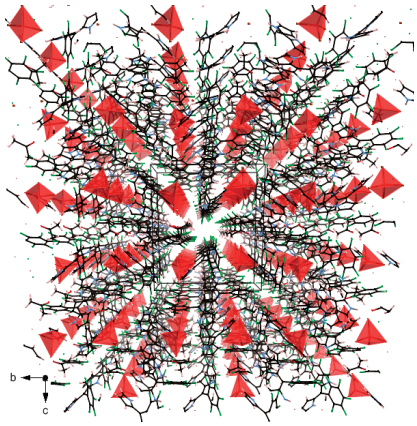

Figure 9. 3D packing diagram of **11**.

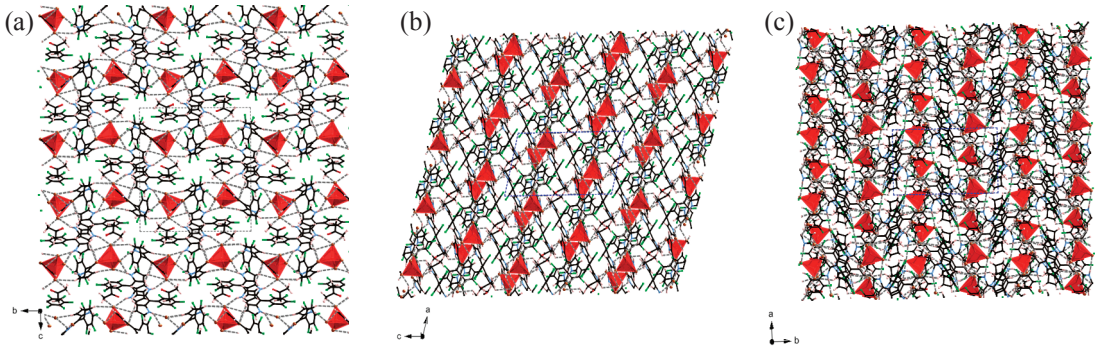

Figure 10. Packing diagrams of **11** through each side; (a) bc, (b) ac, and (c) ab planes. Hydrogen-bonds have been displayed as dotted lines.

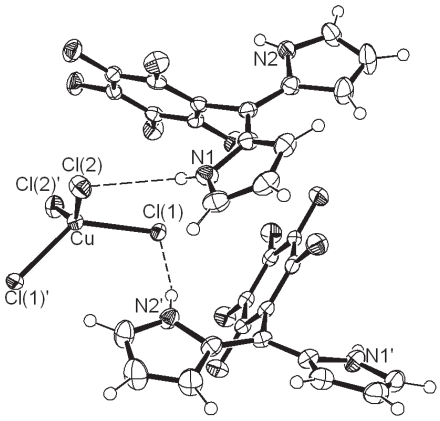

Figure 11. ORTEP structure of **12**.

halides (HF, HCl, and HBr), new self-assemblies of protonated dipyrrins were obtained: $ZnCl_4(HD)_2$ **10**, $ZnBr_4(HD)_2$ **11**, $CuCl_4(HD)_2$ **12**, $CuBr_4(HD)_2$ **13**, $NiBr_4(HD)_2$ **14** and HDBr **15**. The structures of **10**-**12** and **15** were also determined by X-ray diffraction crystallography and exhibit film-like (Figures 7, 10, and 14) and ribbon-like (Figure 16) self-assemblies in the solid state. These self-assemblies employ the type **II** conformations of the dipyrrin units. Self-assemblies taking the type **III** conformation in the solid state remained elusive until we solved the crystal structure for **16**.[29] Figure 17 shows the quinolate units form hydrogen-bonds with two different protonated dipyrrins on each oxygen, and the dipyrrin units display the type **III** conformation. The structural details of self-assemblies utilizing all three dipyrrin conformations are reported in this paper. Furthermore, uni-

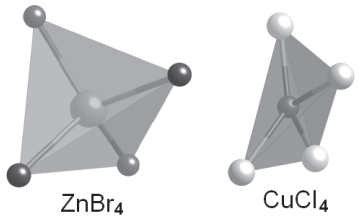

Figure 12. Tetrahedral structural comparison between $ZnBr_4$ and $CuCl_4$ in the corresponding crystals.

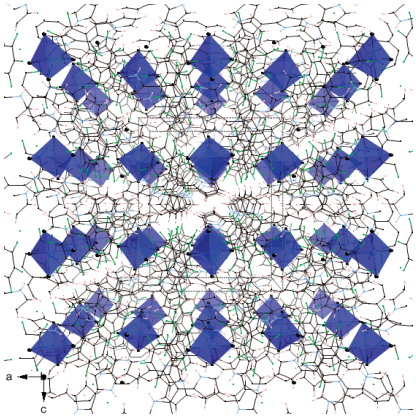

Figure 13. 3D packing diagram of **12**.

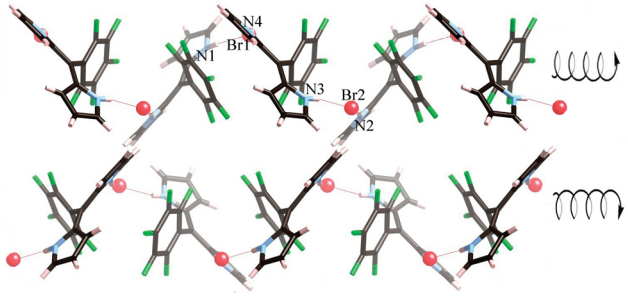

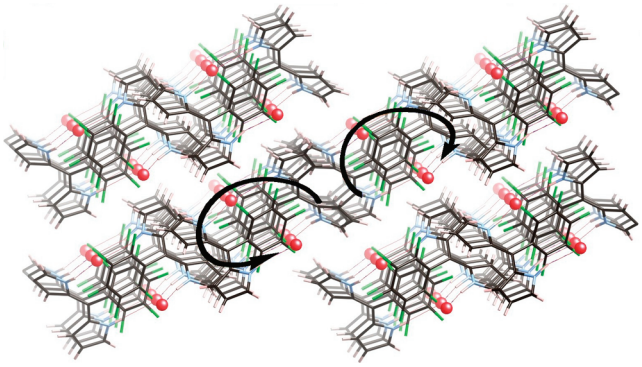

Figure 16. 3D packing diagrams of **15**.

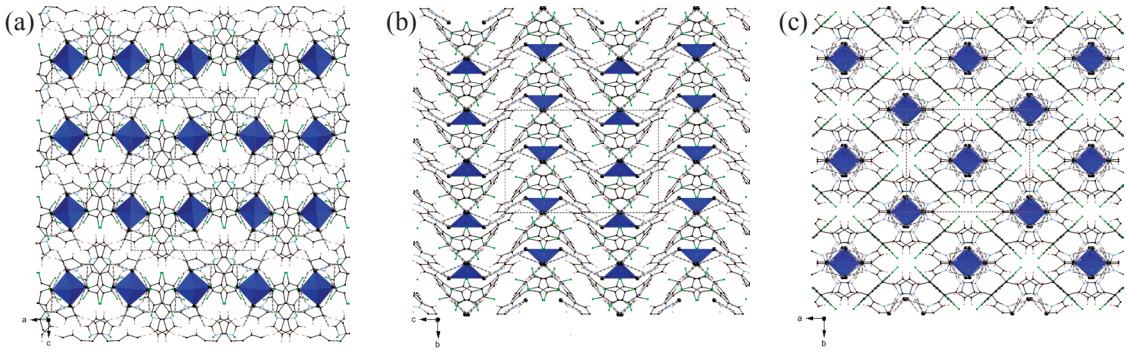

Figure 14. Packing diagrams of **12** through each side; (a) ac, (b) bc, and (c) ab planes. Hydrogen-bonds have been displayed as dotted lines.

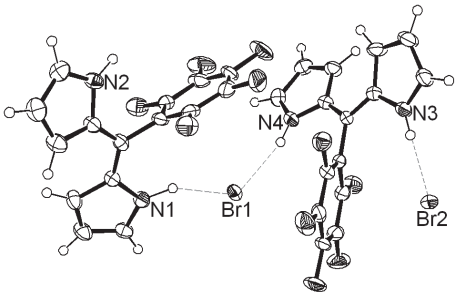

Figure 15. ORTEP structure[28] of **15**.

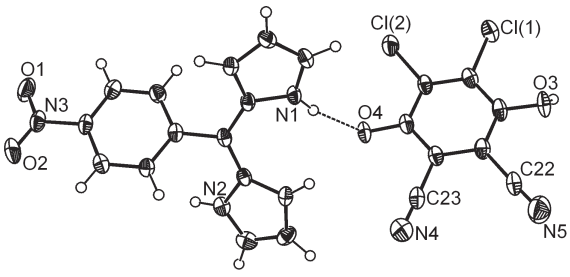

Figure 17. ORTEP structure[29] of **16**.

que "tubular-bunched" arrangements (through long-range hydrogen-bonding) of these self-assemblies were observed with scanning tunneling microscopy (STM).

Experimental

General. All chemicals were purchased from commercial suppliers and used without further purification. Column chromatography of all products was carried out using silica gel (particle size: 0.040 - 0.063 mm, 230 - 400 mesh). ^{1}H and ^{13}C NMR spectra were recorded with Bruker Avance 300 and 400 NMR spectrometers in CD_2Cl_2, $CDCl_3$, d_6-acetone, or d_6-DMSO. Mass spectra were determined on EI, ESI or MALDI-TOF mass spectrometers. Optical spectra were recorded with a Cary 5000 UV-vis spectrophotometer using a 1 cm cell. FTIR spectra were recorded using their KBr pellets.

Preparation of compounds 1-4. Compounds **1-2** were prepared following the literature method.[30] By treatment of the CH_2Cl_2 solutions of **1** and **2** with DDQ, compounds **3-4** were prepared quantitatively. Spectral data of **1**: (67% yield, white powder) mp 127 ~ 128 °C; ^{1}H NMR at rt ($CDCl_3$, 300 MHz) δ 8.08 (bs, 2H), 6.71 (m, J = 1.5, 2H), 6.15 (dd, J = 2.8, dd, J = 6.0, 2H), 6.01 (s, 2H). Spectral data of **2**: (42% yield, light yellow powder) mp 167 °C; ^{1}H NMR at rt ($CDCl_3$, 300 MHz) δ 8.15 (d, J = 8.8, 2H), 7.95 (bs, 2H), 7.35 (d, J = 8.4, 2H); *m/z* EI 145 (75%, $[M\text{-}C_6H_4NO_2]^+$), 201(27%, $[M\text{-}C_4H_4N]^+$), 267 (100%, M^+); Elemental analysis (%) Calcd. 15.94(N), 68.31(C), 4.42(H) found 15.84(N), 67.92(C), 4.18(H). Spectral data of **3**: (reddish powder) ^{1}H NMR at rt ($CDCl_3$, 300 MHz) δ 12.7 (bs, 1H), 7.71 (s, 2H), 6.52 (d, J = 4.2, 2H), 6.46 (dd, J = 4.3, dd, J = 1.4, 2H), ^{19}F NMR (CD_2Cl_2, 282.4 MHz) δ −139.96 (dd, J =19.8, dd, J = 5.6, 2F, o-F), −153.60 (m, 1F, p-F), −162.14 (dt, J = 19.8, dt, J = 5.6, 2F, m-F). Spectral data of **4**: (reddish powder) mp 120 °C; λ_{max} (CH_2Cl_2)/nm 438.0; ^{1}H NMR at rt (CD_2Cl_2, 300 MHz) δ 12.95 (bs, 1H), 8.31 (d, J = 8.8, 2H), 6.49 (dd, J = 4.2, dd, J = 1.0, 2H); ^{13}C NMR (CD_2Cl_2, 75.5 MHz) δ 148.8, 145.1, 144.3, 140.9, 139.3, 132.2, 128.7, 123.4, 118.9; HR ESI calcd. 266.0930 *m/z* (for $C_{15}H_{12}N_3O_2$), found 266.0933 *m/z*.

Preparation of metal complexes 5-9. A CH_3CN (100 mL) solution of *meso*-pentafluorophenyl dipyrromethane (350 mg, 1.12 mmole) was placed in a 250 mL round bottom flask. The resulting solution was oxidized for 40 min by addition of DDQ (255 mg, 1.12 mmole), and then quenched with 0.5 mL of triethylamine. 80 mL of MeOH solution of $ZnCl_2$ (84 mg, 618 mmole) was added into the solution, and the reaction was monitored by TLC. After the reaction was completed, the solvent was removed on a rotary evaporator. The residue was purified by column chromatography on silica gel with CH_2Cl_2 and recrystallized from CH_2Cl_2/MeOH to obtain compound **5** in *ca*. 48% yield. Complexes **6-9** were prepared from corresponding metal salts following the same method (*ca*. 13 ~ 20% yields). Spectral data of Zn^{2+} complex **5**: mp > 230 °C; ^{1}H NMR at rt (CD_2Cl_2, 300 MHz) δ 7.59 (s, 4H), 6.70 (d, J = 4.2, 4H), 6.49 (dd, J = 4.2, dd, J = 1.3, 4H); ^{19}F NMR at rt (CD_2Cl_2, 282.4 MHz) δ −63.59 (dd, J = 22.8, dd, J = 6.6, 4F), −77.21 (t, J = 21.9, 2F), −85.45 (tt, J = 22.2, tt, J = 6.3, 4F); ^{13}C NMR at rt (CD_2Cl_2, 75.5 MHz) δ 152.1, 140.0, 131.6, 119.1 (peaks of *meso*-aryl Cs are broaden due to C-F couplings); ν_{max} (KBr)/cm^{-1} 2957.8s, 2919.8s, 2839.1s, 1734.1w, 1557.7m, 1522.3m, 1458.5s, 1378.0s, 1338.0w, 1243.5w, 1165.7w, 1030.6m, 992.9m, 842.0w, 750.8w; UV-vis (CH_2Cl_2) λ_{max}/nm (log ε) 304 (4.1), 370 (4.2), 496 (5.2); LSIMS 682.2 *m/z* (M^+); Elemental analysis (%) Calcd. 8.19(N), 52.69(C), 1.77(H) found 8.31(N), 53.00(C), 1.85(H). Spectral data of Cu^{2+} complex **6**: mp > 230 °C; ν_{max} (KBr)/cm^{-1} 2957.6s, 2920.9s, 2839.5s, 1733.8w, 1560.3w, 1458.4s, 1377.8s, 1165.8m, 998.0w, 973.4w, 814.2w; 8.10 (bs, 2H), LSIMS 682.0 *m/z* (M^+); ν_{max} (CH_2Cl_2, logε)/nm 380 (4.2), 476 (4.8), 512 (4.5). Spectral data of Ni^{2+} complex **7**: mp > 230 °C; ν_{max} (KBr)/cm^{-1} 2958.8s, 2920.9s, 2839.2s, 1734.3w, 1560.7w, 1458.5s, 1378.0s, 1165.7w, 996.9w, 841.7w, 753.5w; LSIMS 677.04 *m/z* (M^+). Spectral data of Mn^{3+} complex **8**: ^{1}H NMR at rt (CD_2Cl_2, 300 MHz) δ 19.31 (bs, 6H), 6.45 (d, J = 18.4, 6H), −31.04 (bs, 6H). Spectral data of Fe^{3+} complex **9**: mp > 230 °C; ^{1}H NMR at rt (d_6-acetone, 300 MHz) δ −6.20 (s, 6H), −7.22 (s, 6H), −28.78 (s, 6H); ^{19}F NMR at rt (d_6-acetone, 282.4 MHz) δ −62.01 (dd, J = 23.7, dd, J = 6.3, 2H), −78.65 (t, J = 21.9, 1H), −86.23 (t, J = 22.2, 2H); ESIMS 984.1 *m/z* (M^+); Elemental analysis (%) Calcd. 8.55(N), 54.96(C), 1.85(H) found 8.61(N), 54.84(C), 1.71(H); λ_{max} (CH_2Cl_2)/nm 450, 500.

Preparation of self-assemblies 10-16. 20 mL of CH_2Cl_2 solution of **5** (90.2 mg, 132 μmole) was placed in a 50 mL round bottom flask, and degassed under nitrogen. 110 μL of 30% HBr solution in acetic acid was added by syringe and the resulting solution was stirred for 6 hr. Precipitates, which appeared during the reaction, were filtered and washed with CH_2Cl_2, hexane, and water. The title compound **11** was obtained in *ca*. 60% yield. Compound **10** was obtained from 35% HCl solution by the same method, and compound **15** was obtained by treating **9** with excess HBr. Self-assemblies **10** and **12-14** were also prepared by the same method using corresponding metal complexes and hydrogen halides (*ca*. 50 ~ 85%); Solubility differences between the metal complexes and the self-assemblies were significant. While the class of metal complexes showed reasonable solubility in CH_2Cl_2, the self-assemblies showed poor solubility in the same solvent. Also, the self-assemblies containing paramagnetic metals resonated broad signals in the regular aromatic region in their NMR spectra, whereas the metal complexes had no such resonance. The dipyrrin resonances are likely less affected by the metal in the self-assemblies by the disruption of direct metal coodination and enhancement of secondary hydrogen-bond formation. Consequently, the mass spectra of the self-assembies showed various patterns of coordination between protonated dipyrrin and metal halide synthons due to the relatively weaker interactions of hydrogen-bonds. Spectral data for $ZnCl_4(HD)_2$ **10**: mp 180 ~ 182 °C; ^{1}H NMR at 360 K (d_6- DMSO, 300 MHz) δ 8.08 (s, 2H), 7.36 (bs, 2H), 6.75 (s, 2H); ^{19}F NMR at 210 K (d_6-acetone, 282.4 MHz), δ −61.78 (d, J = 23.7, 2F, o-F of first component), −62.86 (d, J = 19.8, 2F, o-F of second component), −65.55 (m, 2F, o-F of third component), −75.62 (m, 1F, p-F of first component), −74.8 (m, 1F, p-F of second component), −77.6 (m, 1F, p-F of third component), −85.22 (t, J = 19.5, m-F of first component), −85.53 (t, J = 22, 2F, m-F of second component), −85.92 (m, 2F, m-F of third component); ν_{max} (KBr)/cm^{-1} 2959s, 2920s, 2839m, 1735w, 1504w, 1456s, 1377s, 1332m 1141m, 1046s, 997m, 972m, 868w, 836w, 773w; TOF ES+ 792.9 *m/z* ($[M\text{-}Cl]^+$); Elemental analysis (%) Calcd. 6.75

(N), 43.43(C), 1.94(H), found 6.69(N), 43.69(C), 1.89(H). Spectral data for $ZnBr_4(HD)_2$ **11**: mp 220 ~ 226 °C; ^{1}H NMR at 333 K (d_6-DMSO, 300 MHz) δ 8.17 (s, 2H), 7.49 (br s, 2H), 6.83 (s, 2H); ^{19}F NMR at 330 K (d_6-DMSO, 282.4 MHz), δ −63.98 (bs, 2F), −75.38 (bs, 1F), −85.07 (m, 2F); ν_{max}(KBr)/cm^{-1} 2955s, 2921s, 2839m, 1733w, 1561w, 1503w, 1457s, 1378s, 1332w, 1140w, 1047m, 998m, 973m, 839w; TOF ES+ 926.8 *m*/*z* ([M-Br]$^+$); Elemental analysis (%) Calcd. 5.56(N), 35.74(C), 1.60 (H), 31.72(Br) found 5.34(N), 35.51(C), 1.52(H), 31.43(Br) λ_{max} (CH_2Cl_2, logε)/nm 478 (4.6). Spectral data for $CuCl_4(HD)_2$ **12**: TOF ES+ 1030.1 *m*/*z* ([M+ H_2CuBr_4]$^+$; detected using the single crystals). Spectral data for $CuBr_4(HD)_2$ **13**: mp 187 ~ 189 °C; ^{1}H NMR at rt (d_6-DMSO, 400 MHz) δ 13.06 (bs, 2H, NH), 8.31 (bs, 2H), 8.00 (bs, 2H), 6.96 (bs, 2H); ν_{max} (KBr)/cm^{-1} 2958s, 2921s, 2839m, 1734w, 1560w, 1458s, 1378s, 1166m, 998w, 973w, 841w; TOF ES+ 1021.3 *m*/*z* ([M+Na]$^+$). Spectral data for $NiBr_4(HD)_2$ **14**: mp > 230 °C; ^{1}H NMR at rt (d_6-DMSO, 400 MHz) δ 13.05 (bs, 2H), 8.28 (bs, 2H), 8.10 (bs, 2H), 6.94 (bs, 2H); ν_{max}(KBr)/cm^{-1} 2957s, 2921s, 2840m, 1734w, 1459s, 1378s, 1166m, 998w, 974w, 841w; TOF ES+ 685.1 *m*/*z* ([M-D]$^+$). Spectral data for HDBr **15**: mp > 230 °C; ^{1}H NMR at rt ($CDCl_3$, 300 MHz) δ (ppm) 7.10 (br s, 1H), 7.03 (br s, 3H), 6.76 (d, 1H, *J* = 2.1), 6.50 (d, 1H, *J* = 2.1); ^{19}F NMR at 243 K (d_6-acetone, 282.4 MHz), δ −65.133 (d, *J* = 48.9, 2H, o-F,), −78.775 (t, *J* = 24.6, 1F, p-F), −86.402 (tt, *J* = 22.5, tt, *J* = 5.7, 2F, m-F,); TOF ES+ 311 *m*/*z* ([M-Br]$^+$); λ_{max} (CH_2Cl_2)/nm 314, 476. **16** was prepared by DDQ oxidation of **2** in the presence of HCl. Spectral data for **16**: mp > 230 °C; λ_{max} (CH_2Cl_2)/nm 470; ^{1}H NMR at 333 K (d_6-acetone, 300 MHz) δ 8.36 (d, *J* = 8.8, 2H), 7.77 (s, 2H), 7.76 (d, *J* = 8.7, 2H), 6.50 (d, *J* = 4.1, 2H), 6.42

Table 1. Selected crystallographic data of **3**-**6** and **8**-**9**.

	3	**4**[29]	**5**	**6**	**8**	**9**
A. Crystal Data						
Formula	$C_{15}H_7N_2F_5$	$C_{15}H_{11}N_3O_2$	$C_{30}H_{12}F_{10}N_4Zn$	$C_{30}H_{12}F_{10}N_4Cu$	$C_{45}H_{18}N_6F_{15}Mn$	$C_{45}H_{18}N_6F_{15}Fe$
Mw	310.23	265.27	683.81	681.98	982.59	983.50
Cryst. Color, habit	dark, needle	red, prism	red, plate	red, plate	shiny green, irregular	Red, platelet
Cryst. dimensions (mm)	0.40×0.20×0.20	0.35×0.25×0.12	0.25×0.13×0.05	0.30×0.15×0.03	0.15×0.10×0.10	0.25×0.12×0.03
Cryst. System, Lattice type	Orthorhombic	Orthorhombic	Monoclinic	Monoclinic	Monoclinic	Monoclinic
Space group	$P2_12_12_1$(#19)	*Pbca* (# 61)	*C*2/*c* (# 15)	$P2_1/c$ (#14)	$P2_1/n$ (# 14)	$P2_1/n$ (# 14)
a (Å)	8.9173(6)	14.6809(16)	55.915(9)	15.450(2)	10.3595(5)	10.2500(15)
b (Å)	9.1568(6)	7.4146(9)	8.176(2)	9.1389(9)	13.5804(9)	13.6111(19)
c (Å)	15.3482(10)	24.350(3)	12.195(2)	19.725(2)	26.6890(19)	27.829(4)
(deg)	90	90	92.900(10)	112.500(10)	94.098(3)	94.546(4)
V (Å^3)	1253.24(14)	2650.6(6)	5567.9(19)	2573.1(5)	3745.2(4)	3870.3(10)
Z	4	8	8	4	4	4
D_c(g/cm^3)	1.644	1.329	1.631	1.760	1.743	1.688
F_{000}	624.00	1104.00	2720.00	1356.00	1960.00	1964.00
μ(Mo Kα) (mm^{-1})	0.151	0.092	0.978	0.952	0.474	0.507
B. Intensity Measurements						
Diffractometer	Rigaku/ADSC CCD	Bruker X8 APEX	Rigaku/ADSC CCD	Rigaku/ADSC CCD	Bruker X8 APEX	Rigaku/ADSC CCD
Total No. of refl. measured	11430 (R_{int} = 0.053)	54647 (R_{int} = 0.0325)	22844 (R_{int} = 0.061)	23088 (R_{int} = 0.0814)	65695 (R_{int} = 0.0646)	29858 (R_{int} = 0.124)
Corrections	0.769 ~ 0.970	0.941 ~ 0.989	0.550 ~ 0.952	0.690 ~ 0.972	0.0815 ~ 0.954	0.815 ~ 0.985
C. Structure Solution and Refinement						
Structure solution	Direct methods (SIR92)	Direct methods (SIR92)	Direct methods (SIR92)	Direct methods (SIR92)	Direct methods (SIR92)	Patterson methods (DIRDIF92 PATTY)
No. observation ($I > 0.00\sigma(I)$)	2696	3122	6020	5293	7314	6779
No. variables	203	185	407	406	604	605
Refl./para. ratio	13.28	16.88	14.79	13.04	12.11	11.20
R1; *wR2*	0.0407; 0.0622	0.0621; 0.1160	0.1374; 0.2200	0.1067; 0.1359	0.0587; 0.1076	0.1273; 0.1670
R1; *wR2*	0.0292; 0.0588	0.0403; 0.1051	0.0890; 0.1855	0.0556; 0.1203	0.0388; 0.1006	0.0607; 0.1238
GOF	0.904	1.074	0.883	0.964	1.080	0.830

(dd, J = 4.4, ^{dd}J = 1.5, 2H); HR ESI (+) calcd. 266.0930 m/z (for $C_{15}H_{12}N_3O_2$), found 266.09028 m/z, (-) calcd. 226.9415 m/z (for $C_8HN_2O_2{}^{35}Cl_2$), found 226.9423.

STM determination of the self-assemblies 11 and 13-14. For adsorption of the self-assemblies **11** and **13-14** onto a graphite surface (MikroMasch, grade ZYA), the compound was first dissolved in methanol at a concentration of *ca.* 1.0×10^{-5} M. A drop of the solution was placed onto a freshly cleaved surface and left to dry in air either at room temperature or at 100 °C for several hours. The drops spread evenly over the surface, resulting in uniform coverage of the entire surface with each compound. STM topographical images were obtained using a scanning tunneling microscope (SOLVER P-47, NT-MDT) under ambient conditions. STM tips were mechanically cut from a 0.25 mm Pt/Ir wire and tunneling currents between 30 and 60 pA were employed. The sample bias voltage and the scan frequency were 100 to 200 mV and between 0.5 and 3 Hz, respectively. Constant-current mode was employed to investigate the static properties of the structures. Multiple-tip effects, which can produce misleading features in STM images, were removed by a repeated tip sharpening process *in situ* at a graphite step edge. All of the images shown are raw data with mean plane subtraction to reduce the thermal drift effect.

Results and Discussion

Dipyrrins become more stable when substituted with electron-withdrawing groups and more conformationally mobile when unsubstituted in the β-positions such as with compounds **3** and **4**. Dipyrromethanes **1** and **2** were prepared following the literature method from free pyrrole and perfluorobenzaldehyde (or 4-nitrobenzaldehyde for **2**) and oxidized using 2,3-dichloro-5,6-dicyano-1,4-benzoquinone (DDQ) to obtain **3** and **4**. Metal complexes **5-9** were simply prepared by treatment of a CH_3CN solution of dipyrrin **3** with MeOH solutions of Zn^{2+}, Cu^{2+}, Ni^{2+}, Mn^{3+} and Fe^{3+} chloride salts. Single crystals of **3-6** and **8-9** were grown by the vapor diffusion of hexane into CH_2Cl_2 solutions and each structure was defined by X-ray diffraction analysis.

Table 2. Selected crystallographic data of **10-13** and **15-16**.

	10[28]	**11**[28]	**12**	**15**[28]	**16**[29]
A. Crystal Data					
Formula	$C_{30}H_{16}Cl_4ZnN_4F_{10}$	$C_{30}H_{16}N_4F_{10}ZnBr_4 \cdot C_3H_6O$	$C_{30}H_{16}Cl_4CuN_4F_{10}$	$C_{15}H_8N_2F_5Br$	$C_{23}H_{13}N_5O_4Cl_2$
Mw	829.66	1065.54	827.81	391.14	494.28
Cryst. Color, habit	red, platelet	blue, block	dark, irregular	red, chip	red, plate
Cryst. dimensions (mm)	0.50×0.30×0.08	0.50×0.20×0.20	0.30×0.20×0.12	0.50×0.25×0.13	0.35×0.10×0.03
Cryst. System, Lattice type	Orthorhombic, primitive	Monoclinic, primitive	Orthorhombic, primitive	Triclinic,	Monoclinic, primitive
Space group	Pbcn(#60)	$P2_1/n$ (# 14)	Pbcn (# 60)	$P\bar{1}$ (# 2)	$P2_1/n$ (# 14)
a (Å)	14.6458(6)	10.4590(7)	14.818	8.2509(2)	10.508(2)
b (Å)	11.9140(6)	18.2100(9)	11.405	10.9918(1)	19.587(3)
c (Å)	18.0743(9)	20.058(1)	18.408	17.5200(6)	11.039(2)
(deg)	90	105.072(2)	90	79.310(9) *	107.970(10)
V (Å^3)	3153.8(4)	3688.8(3)	3110.9	1480.7(1)	2161.2(7)
Z	4	4	4	4	4
D_c(g/cm^3)	1.747	1.919	1.767	1.754	1.519
F_{000}	1648.00	2064.00	1644.00	768.00	1008.00
μ(MoKα) (cm^{-1})	1.207	5.097	1.137	2.838	0.344
B. Intensity Measurements					
Diffractometer	Rigaku / ADSC CCD	Bruker X8 APEX	Bruker X8 APEX	Rigaku / ADSC CCD	Bruker X8 APEX
Total No. of refl. measured	28992 (R_{int} = 0.05940)	33094 (R_{int} = 0.05739)	32908 (R_{int} = 0.0372)	13327 (R_{int} = 0.04372)	34997 (R_{int} = 0.0710)
Corrections	0.7515 ~ 1.0000	0.6906 ~ 1.0000	0.471 ~ 0.711	0.7733 ~ 1.0000	0.756 ~ 0.990
C. Structure Solution and Refinement					
Structure solution	Patterson methods (DIRDIF92 PATTY)	Direct methods (SIR 97)	Direct methods (SIR 92)	Direct methods (SIR 97)	Direct methods (SIR 92)
No. observation ($I > 0.00\sigma(I)$)	3476	8221	3715	6074	3842
No. variables	230	494	230	427	319
Refl./para. ratio	15.11	16.64	16.15	14.22	12.04
$R1$; $wR2$	0.0486; 0.0700	0.0585; 0.0963	0.0560; 0.0801	0.0799; 0.1493	0.0756; 0.1290
$R1$; $wR2$	0.027; 0.0700	0.031; 0.035	0.0310; 0.0701	0.043; 0.059	0.0456; 0.1087
GOF	0.926	0.842	1.047	1.131	1.09

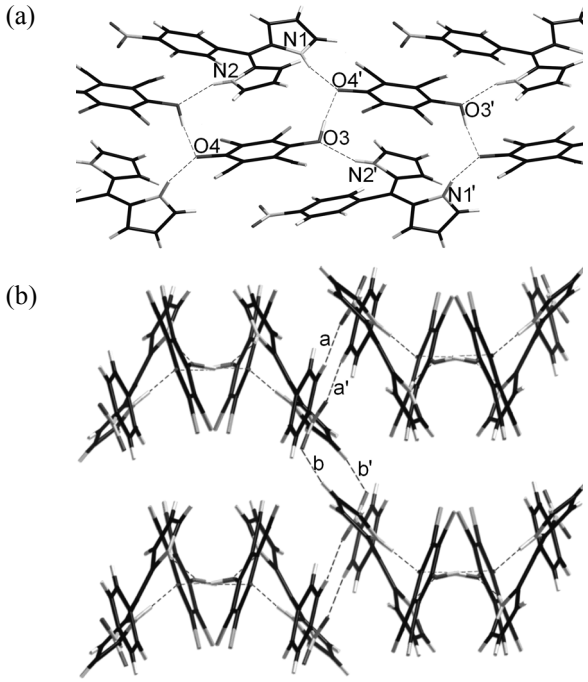

Figure 18. 3D packing diagrams of **16**; [(a) top view and (b) side view] showing the hydrogen-bonding system between protonated dipyrromethene and deprotonated/reduced DDQ; hydrogen-bonds are denoted by dotted red (OH···O), blue (NH···O), and black (CH···O) lines.

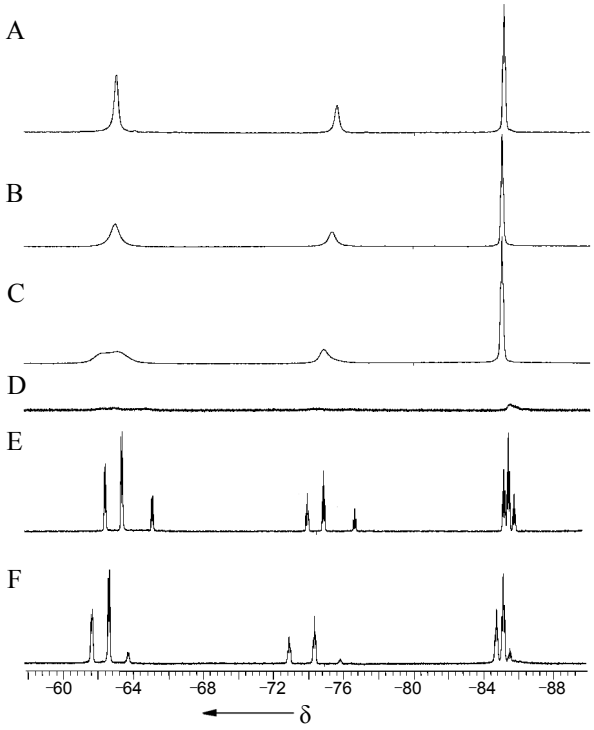

Figure 19. Variable temperature ^{19}F NMR spectra of **11** in d_6-DMSO (A-C) and d_6-acetone (D-F); (A) 353 K, (B) 333K, (C) 300 K, (D) 300 K, (E) 253 K, and (F) 223 K.

As shown in Figures 3 and 4, the ZnD_2 **5** and CuD_2 **6** have tetrahedral structures while MnD_3 **8** (Figure 4a) and FeD_3 **9** (Figure 4b) have octahedral coordinations. ZnD_2 **5** shows a *ca*. 45° dihe-

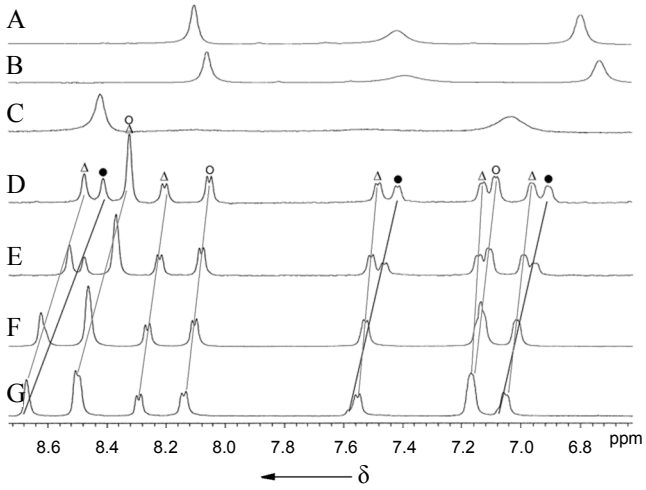

Figure 20. Various temperature 1H NMR spectra of **11** in d_6-DMSO (A-B) and d_6-acetone (C-G); (A) 353 K, (B) 333K, (C) 300 K, (D) 253 K, (E) 223 K, (F) 203 K, and (G) 183; ○ conformation I, ● conformation **II**, and ▲conformation **III**.

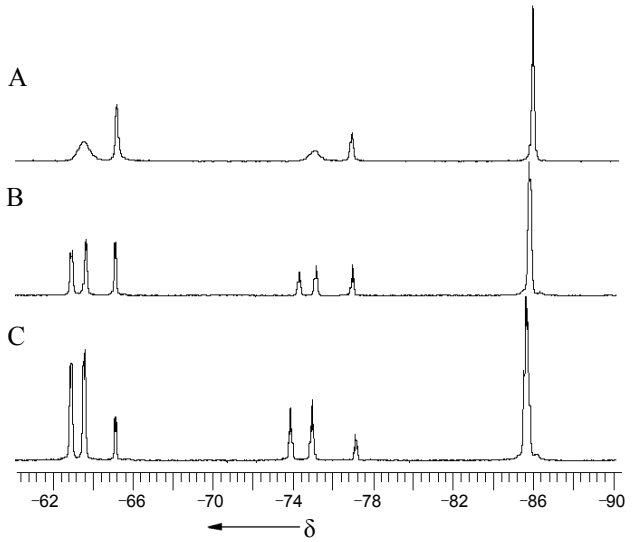

Figure 21. Variable temperature ^{19}F NMR spectra of **15** in d_6-acetone; (A) 300 K, (B) 260K, and (C) 220 K.

dral angle for the planes along the two chelating dipyrrin ligands and the same angle is 60° for CuD_2 **6**. As shown in the selected crystallographic data in Table 1, all the single crystals of the metal complexes have monoclinic systems. The NMR spectra of the metal complexes **6-9** exhibit signals over a large chemical-shift range or completely disappeared due to the paramagnetism of the metal centers while the diamagnetic Zn complexes **5** shows typical chemical shifts in their NMR spectrum. As reported in previously,[31-33] the optical spectra of the metal complexes showed strong absorption bands newly appearing along with metal complexation. Similarly, the optical spectrum of the trivalent metal complexes **8** and **9** are also dramatically changed from that of the ligand. Relatively numerous splittings of molecular orbitals by increasing the ligation number caused the absorption bands to be slightly broadened and weaker compared to the divalent metal complexes.

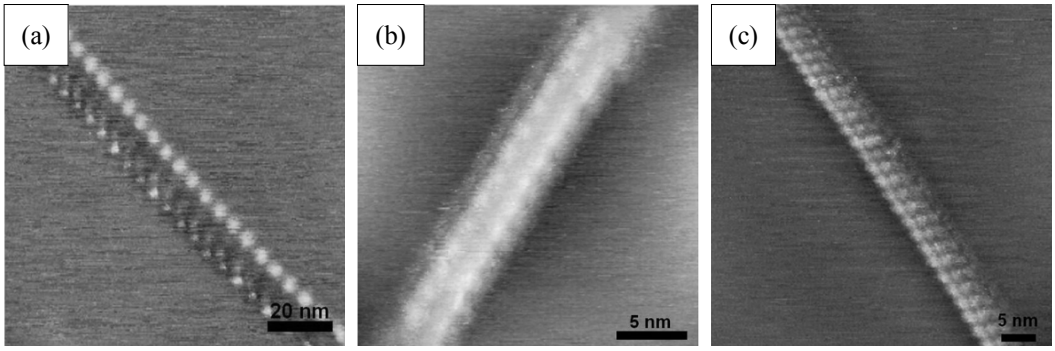

Figure 22. STM patterns for **11** (a), **13** (b), and **14** (c).

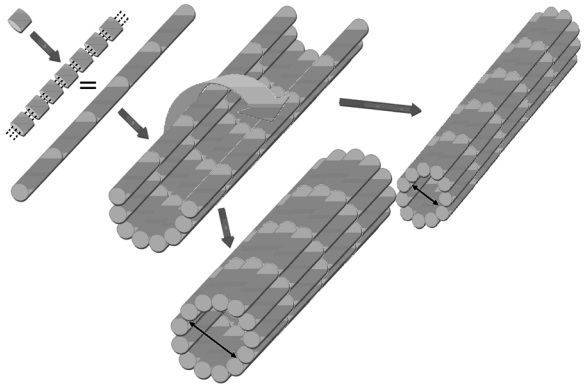

Figure 23. Graphic displays for the explanation of tubular formations.

As shown in Figure 1, dipyrrin can exhibit three possible conformations. Conformation **I** is observed in the general crystal structure of free-based dipyrrins. As shown in Figure 2, the crystal structures of **3** and **4** show the stable type I conformation formed *via* intramolecular hydrogen-bonding between imino-N and amino-NH. Similarly, general metal complexes of dipyrrin ligands takes conformation **I** by clamping both the imino- and amino-N atoms by the central metals (Figures 3 and 4). The self-assemblies containing protonated dipyrrins, $ZnCl_4(HD)_2$ **10**, $ZnBr_4(HD)_2$ **11**, $CuCl_4(HD)_2$ **12**, $CuBr_4(HD)_2$ **13**, $NiBr_4(HD)_2$ **14**, and HDBr **15** were formed when hydrogen halides (HCl for **10** and **12**, HBr for **11** and **13**-**15**) were added to CH_3CN solutions of **5**-**9**. Each single crystal was obtained by slow evaporation of a solution in water and methanol and the structures of the self-assemblies **10**-**12** and **15** were defined by X-ray diffraction analysis. The single crystals are hygroscopic and readily become viscous and amorphous and dark color.

As shown in Figures 5, 8, 11, and 15, the initial conformation of the dipyrrin components were converted to the type **II** conformation. Introduction of halide anions caused the cleavage of the original metal-N bonds and led to formation of new metal-halide bonds. The metal tetrahalide (ML_4) complexes were the first species formed within this motif. Additionally, the dipyrrin molecules were protonated during the treatment with hydrogen halide (HL). The ML4s are dianions and the resulting self-assemblies have a net charge of zero when generated with two protonated-dipyrrins (HDs), where the positive charges are delocalized throughout the entire aromatic dipyrrin. Similarly, the negative charge is also delocalized through the ML_4 units. The four halide arms of ML_4s which can generate four different hydrogen-bonds, link with four dipyrrin components (two protonated NHs and two original amino-NHs). As a result, the superstructure assembly generated through hydrogen-bonding interactions has zero net-charge. These co-crystals also exhibit rather unique multi-dimensional arrangements. As shown in Figures 6, 9 and 13, the three-dimensional packing diagrams display complicated but well-repeated patterns. Within the continuously repeating hydrogen-bonding network, the two-dimensionally aligned molecules are tightly linked with each other and the final structures occur as two dimensional layered superstructures. The side views of the alignments help in recognizing the individual superstructural layers (Figures 7, 10 and 14, especially the individual super-structural layer denoted in Figure 7 (c), as an example). The molecular arrangements in the self-assemblies are very similar, but the distances between each layer are due to the differences in the van der Waals bond distances and the dihedral angle of the ML_4 tetrahedral units. $CuCl_4$ components in the crystal exhibited a more distorted tetrahedral coordination than $ZnBr_4$ (Figure 12).

Self-assembly (Figure 15) of HD and a bromide anion shows ribbon-like molecular arrangements as a result of the hydrogen-bonding networks. Interestingly, it is a racemic mixture having two different helical structures as denoted with black arrows in Figure 15. As mentioned above, the type **I** and **II** conformations were well represented in the various solid states. On the other hand, the type **III** conformation (Figure 1) was as yet unknown until the crystal structure of compound **16** (Figure 17) was determined.

The single crystal of **16** was obtained by evaporation of a solution of methanol and trace HCl in water. The crystal structure as presented in Figures 17 and 18(a) contains a dipyrrin component in an asymmetric type **III** conformation. Similar to the previous self-assemblies, the dipyrrin units in the crystal were protonated. A crystal of HDs and deprotonated diquinolate components was formed in the presence of acid. The structure of the self-assembly was tightened by three different types of hydrogen-bonds, O-H···O (1.53 Å), N-H···O (1.85 and 2.01 Å) and C-H···O (2.59 and 2.71 Å).[29]

As shown in the crystal structures above, the conformational differences of the three dipyrrins were confirmed in the solid

state. In order to examine conformational changes in solution NMR spectral analysis at various temperatures was utilized. Figure 19 shows the various temperature ^{19}F NMR spectra of **11**. At higher temperatures, the spectrum showed the presence of one conformer. As the temperature was lowered, the peaks progressively broadened and split. As shown in spectrum D (d_6-acetone solution), the F-peaks almost disappeared at room temperature. With continued lowering of the temperature, the F-signals reappeared showing all three different conformation types. One can confidently distinguish each set of peaks of the three conformations from the temperature dependence of the ^{1}H NMR spectra of **11** (Figure 20). Similarly, ^{19}F NMR spectra of **15** were considered as a three conformational mixture (Figure 21).

Further investigation of the arrangements of these self-assemblies in both the solid and solution states continued with microscopic analysis. Drops of MeOH solutions of compounds **11** and **13-14** were placed on highly-oriented pyrolytic graphite surfaces (HOPGS) and the solvent was allowed to completely evaporate. The graphite plates were connected to a low-current preamplifier electrode for STM-analysis. The STM images are presented in Figure 22. As shown in Figure 23, the self-assemblies on the graphite surface initially formed one-dimensional arrangements *via* the specific interactions of the components, which might be considered as hydrogen-bonds as described above. The 1D-aligned assembly continuously interacts with another 1D-aligned unit to form tubular bunches. These tubular structures might well be in accordance with the supermolecular layered structures of the crystals reported above. The STM image in Figure 22(a) likely represents a case where the alignment was stopped before completing the tubular arrangement.

Conclusion

Three possible conformations of dipyrrins, which are shown as type **I**, **II** and **III** in Figure 1, have been observed in both the solid and solution states. The crystals of free-base dipyrrin and metal-dipyrrin complexes reveal type **I** conformation. Alternately, self-assemblies built *via* metal-N bond cleavage followed by new coordinate-bond generation to produce metal tetrahalides, protonation of imino-nitrogen, and hydrogen-bond formation between halide atoms and NH groups showed type **II** conformation. The co-crystalline structure of self-assembly **16** provided the last conformation, type **III**. Additionally, the three conformations were observed in solution using variable-temperature NMR. The layered arrangements of the self-assemblies generated tubular bunches on a HOPGS as shown *via* STM.

Studies on alternative dimensional arrangements using self-assemblies built by diverse combinations of flexible components are ongoing.

Acknowledgments. This work was supported by the Natural Sciences and Engineering Research Council (NSERC) of Canada. SBS and JRH thank the KOSEF funded by the MOST (R11-2007-012-02001-0 and R01-2007-000-20237-0).

References

1. Desiragu, G. R. *Crystal Engineering: The Design of Organic Solids*; Elsevier: Amsterdam, 1989.
2. Lehn, J. M. *Supramolecular Chemistry: Concepts and Perspectives*; VCH: Weinheim, 1995.
3. *Comprehensive Supramolecular Chemistry*; Atwood, J. L., Davies, J. E. D., MacNicol, D. D., Vogtle, F., Eds.; Pergamon: Oxford, 1996.
4. Desiraju, G. R. *Nature* **2001**, *412*, 397.
5. Hollingsworth, M. D. *Science* **2002**, *295*, 2410.
6. MacDonald, J. C.; Dorrestein, P. C.; Pilley, M. M.; Foote, M. M.; Lundburg, J. L.; Denning, R. W.; Schultz, A. J.; Manson, J. L. *J. Am. Chem. Soc.* **2000**, *122*, 11692.
7. Moulton, B.; Zaworotko, M. J. *Chem. Rev.* **2001**, *101*, 1629.
8. Sommerdijk, N. A. J. M. *Angew. Chem. Int. Ed.* **2003**, *42*, 3572.
9. Daisuke, U.; Yusuke, U.; Takashi, O. *Science* **2009**, *326*, 120-123.
10. Yaghi, O. M.; O'Keeffe, M.; Ockwig, N. W.; Chae, H. K.; Eddaudi, M.; Kim, J. *Nature* **2003**, *423*, 705-714.
11. Ko, Y. H.; Kim, E.; Hwang, I.; Kim, K. *Chem. Commun.* **2007**, 1305-1315.
12. Sharma, C. V. K.; Broker, G. A.; Huddleston, J. G.; Baldwin, J. W.; Metzger, R. M.; Rogers, R. D. *J. Am. Chem. Soc.* **1999**, *121*, 1137.
13. Yanagi, H.; Mukai, H.; Ikuta, K.; Shibutani, T.; Kamikado, T.; Yokoyama, S.; Mashiko, S. *Nano Lett.* **2002**, *2*, 601.
14. Chen, Q.; Dolphin, D. *Can. J. Chem.* **2002**, *80*, 1668.
15. Thompson, A.; Rettig, S. J.; Dolphin, D. *Chem. Commun.* **1999**, 631.
16. Zhang, Y.; Thompson, A.; Rettig, S. J.; Dolphin, D. *J. Am. Chem. Soc.* **1998**, *120*, 13537.
17. Maeda, H.; Mihashi, Y.; Haketa, Y. *Org. Lett*. **2008**, *10*, 3179.
18. Maeda, H. *Eur. J. Org. Chem.* **2007**, 5313.
19. Sessler, J. L.; Berthon-Gelloz, G.; Gale, P. A.; Camiolo, S.; Anslyn, E. V.; Anzenbacher, P., Jr.; Furuta, H.; Kirkovits, G. J.; Lynch, V. M.; Maeda, H.; Morosini, P.; Scherer, M.; Shriver, J.; Zimmerman, R. S. *Polyhedron* **2003**, *22*, 2963.
20. Sessler, J. L.; Jayawickramarajah, J.; Sherman, C. L.; Brodbelt, J. S. *J. Am. Chem. Soc.* **2004**, *126*, 11460.
21. Katayev, E. A.; Boev, N. V.; Khrustalev, V. N.; Ustynyuk, Y. A.; Tananaev, I. G.; Sessler, J. L. *J. Org. Chem.* **2007**, *72*, 2886.
22. Desiraju, G. R. *Angew. Chem. Int. Ed. Engl.* **1995**, *34*, 2311.
23. Desiraju, G. R. *Chem. Commun.* **1997**, 1475.
24. Bond, A. D. *CrystEngComm.* **2007**, *9*, 833.
25. Simard, M.; Su, D.; Wuest, J. D. *J. Am. Chem. Soc.* **1991**, *113*, 4696.
26. Fournier, J. H.; Maris, T.; Wuest, J. D.; Guo, W. Z.; Galoppini, E. *J. Am. Chem. Soc.* **2003**, *125*, 1002.
27. Falk, H. In *The Chemistry of Linear Oligopyrroles and Bile Pigments*; Springer-Verlag Wien: New York, 1989; pp 108.
28. Shin, J. Y.; Dolphin, D.; Patrick, B. O. *Cryst. Growth Des.* **2004**, *4*, 659.
29. Shin, J. Y.; Patrick, B. O.; Dolphin, D. *CrystEngComm.* **2008**, *10*, 960.
30. Shin, J. Y.; Patrick, B. O.; Dolphin, D. *Org. Biomol. Chem.* **2009**, *7*, 2032.
31. Brückner, C.; Karunaratne, V.; Rettig, S.; Dolphin, D. *Can. J. Chem.* **1996**, *74*, 2182.
32. Miao, Q.; Shin, J. Y.; Patrick, B. O.; Dolphin, D. *Chem. Commun.* **2009**, 2541-2543.
33. Brückner, C.; Zhang, Y.; Rettig, S. J.; Dolphin, D. *Inorg. Chim. Acta.* **1997**, *263*, 279-286.